รายงานวิจัยฉบับสมบูรณ์

โครงการพลศาสตร์ของขดคลื่นภายใต้การควบคุมแบบป้อนกลับในปฏิกิริยาเบลูซอฟจาโบทินสกีที่ไวแสง

โดย ผศ. อรอุมา เขียวหวาน และคณะ

รายงานวิจัยฉบับสมบูรณ์

โครงการพลศาสตร์ของขดคลื่นภายใต้การควบคุมแบบป้อนกลับ
ในปฏิกิริยาเบลูซอฟจาโบทินสกีที่ไวแสง

คณะผู้วิจัย	สังกัด
1. ผศ. อรอุมา เขียวหวาน	มหาวิทยาลัยมหิดล
2. รศ. ประพิณ วิไลรัตน์	มหาวิทยาลัยมหิดล
3. Prof. Stefan C. Müller	Otto-von-Guericke Universität

พลศาสตร์ของขดคลื่นภายใต้การควบคุมแบบป้อนกลับในปฏิกิริยาเบลูซอฟจาโบทินสกีที่ไวแสง

อรอุมา เขียวหวาน, สุพิชชัย กาญตระศิริ, ชนเนษฎ์ อุทัยสาร์, ประพิณ วิไลรัตน์, สเตฟาน ซี มีลเลอร์

ภาควิชาเคมี คณะวิทยาศาสตร์ มหาวิทยาลัยมหิดล ถนนพระราม 6 เขตพญาไท กรุงเทพฯ 10400

Institut für Experimentelle Physik, Otto-von-Guericke-Universität, Universitätsplatz 2, D-39106 Magdeburg, Germany

---

บทคัดย่อ

ในการศึกษาการควบคุมแบบป้อนกลับแบบไม่เฉพาะที่ ขดคลื่นในปฏิกิริยาเบลูซอฟจาโบทินสกีจะถูกฉายด้วยแสงเอกรูปซึ่งมีค่าความเข้มขึ้นกับเวลา โดยมีค่าความเข้มแสงเป็นสัดส่วนโดยตรงกับค่าเฉลี่ยของปริมาณคลื่นเชิงเคมีที่อยู่ภายในโดเมนรูปสี่เหลี่ยมของปฏิกิริยา จากผลการทดลองเราพบว่า พลศาสตร์ของขดคลื่นเปลี่ยนไปอย่างหลากหลายอันเนื่องมาจากการควบคุมแบบป้อนกลับนี้ นั่นคือทำให้เกิดการเคลื่อนที่ของแกนของขดคลื่นเป็นรูปร่างต่างๆ อาทิเช่น รูปสี่เหลี่ยม รูปกากบาท เป็นต้น เรขาคณิตของโดเมนที่ใช้ควบคุมความเข้มแสงมีอิทธิพลสำคัญต่อขนาดและรูปร่างของเส้นทางการเคลื่อนที่ของขดคลื่น ผลการทดลองในห้องปฏิบัติการได้ถูกนำมาศึกษาเพิ่มเติมและยืนยันด้วยการศึกษาในเชิงตัวเลข โดยในกรณีนี้ได้มีการใช้โดเมนที่มีขนาดและรูปร่างที่หลากหลายมากขึ้น ปรากฏการณ์ที่เกิดขึ้นสามารถอธิบายได้ในเชิงทฤษฎี โดยการสร้างแผนที่กระแสของการเคลื่อนที่ของแกนของขดคลื่นจากการวิเคราะห์สัญญาณควบคุม

ในกรณีการควบคุมแบบป้อนกลับเฉพาะที่ ขดคลื่นจะถูกควบคุมโดยการฉายแสงเป็นช่วงสั้นๆ ณ ขณะที่หน้าคลื่นเคลื่อนที่ผ่านจุดที่เรียกว่าจุดวัดที่กำหนดไว้ จากการทดลองพบว่าระยะระหว่างแกนของขดคลื่นและจุดวัดเป็นพารามิเตอร์สำคัญที่กำหนดเส้นทางการเคลื่อนที่ของขดคลื่นซึ่งมีลักษณะเป็นวงโคจร ที่เรียกว่าเรโซแนนซ์แอตแทรกเตอร์ (resonance attractor) โดยถ้าระยะระหว่างแกนของขดคลื่นและจุดวัดมีค่าน้อย การเคลื่อนที่ของขดคลื่นจะเป็นเรโซแนนซ์แอตแทรก-เตอร์แบบไฮโพไซคลอยด์ (hypocycloid) แต่ในทางตรงกันข้ามถ้าระยะมีค่ามาก จะเป็นเรโซแนนซ์แอตแทรกเตอร์แบบอิพิ-ไซคลอยด์ (epicycloid) นอกจากนี้การเพิ่มการหน่วงเวลาเข้าไปในวงจรการควบคุมแบบป้อนกลับจะมีผลให้ขนาดของเรโซ-แนนซ์แอตแทรกเตอร์เปลี่ยนไป สุดท้ายผลการทดลองทั้งในเชิงปฏิบัติการและเชิงตัวเลขได้ถูกนำมาเปรียบเทียบกับทฤษฎีเกี่ยวกับเรโซแนนซ์แอตแทรกเตอร์ที่ถูกนำเสนอก่อนหน้านี้

คำหลัก : ขดคลื่นเชิงเคมี; ปฏิกิริยาเบลูซอฟจาโบทินสกี; การควบคุมแบบป้อนกลับ

Dynamics of Spiral Waves under Feedback Control in the Light-Sensitive Belousov-Zhabotinsky Reaction

On-Uma Kheowan, Supichai Kantrasiri, Chananate Uthaisar, Prapin Wilairat, Stefan C. Müller

Department of Chemistry, Mahidol University, Rama 6 Road, Bangkok 10400, Thailand
Institut für Experimentelle Physik, Otto-von-Guericke-Universität, Universitätsplatz 2, D-39106 Magdeburg, Germany

---

Abstract

For non-local feedback control, spiral waves rotating rigidly in a thin layer of the light-sensitive Belousov–Zhabotinsky (BZ) reaction are subjected to a time dependent uniform illumination. A non-local feedback algorithm computes the illumination intensity to be proportional to the average wave activity within a square-shaped sensory domain. The investigations show a broad spectrum of dynamical responses which results in square- and cross-shaped trajectories of the spiral tip, including reflections at the virtual walls. The geometry of the sensory domain is crucial in determining size and shape of the tip trajectories. The experimental results are complemented by numerical simulations, where the feedback signal is derived from sensory domains with different geometries. A theoretical approach, by constructing a flow map based on an analysis of the feedback signal, is proposed to explain the observed phenomena.

In local feedback, the rigidly rotating spiral waves are investigated under an application of a sequence of short light pulses. Each light pulse is applied at a moment that corresponds to the passage of the wave front through a particular measuring point. For a small distance between the measuring point and the initial location of the spiral core, a resonance attractor with hypocycloidal shape is observed, whereas for a larger distance an epicycloidal resonance attractor occurs. The size of the attractor can be changed by introducing a time delay. Experimental and numerical results are compared with an earlier developed theory on the resonance attractor.

Keywords: Spiral wave; Belousov–Zhabotinsky (BZ) reaction; feedback control

หน้าสรุปโครงการ (Executive Summary)

---

1. ความสำคัญและที่มาของปัญหา

ในช่วงปลายศตวรรษที่ 20 ที่ผ่านมา ได้มีศาสตร์ใหม่ที่มีความสำคัญมากอันหนึ่งเกิดขึ้น นั่นคือ วิชาวิทยาศาสตร์ของระบบที่ไม่เป็นเชิงเส้น (Nonlinear Science) ซึ่งพลศาสตร์ของระบบเหล่านี้มีลักษณะซับซ้อนและคาดเดาได้ยาก ตัวอย่างเช่น ลักษณะการเต้นของหัวใจ การผันแปรของสภาวะอากาศ การขึ้นลงของดัชนีหุ้น รวมไปถึงการเกิดลวดลาย (pattern formation) ในระบบที่ห่างไกลจากสมดุล เช่น ลวดลายที่เกิดขึ้นบนม้าลาย เปลือกหอย เป็นต้น ลวดลายที่น่าสนใจมากชนิดหนึ่งคือ ขดคลื่นลายก้นหอย (spiral wave) ซึ่งพบได้ในธรรมชาติในหลายๆระบบ เช่น การเคลื่อนและจับกลุ่มกันของราเมือกในขณะที่หาอาหาร การหดตัวของกล้ามเนื้อหัวใจในภาวะที่การเต้นของหัวใจล้มเหลว แต่ขดคลื่นลายก้นหอยที่มีผู้ให้ความสนใจศึกษาค้นคว้าและทำการทดลองมากที่สุดคือขดคลื่นเชิงเคมีที่พบในปฏิกิริยาเบลูซอฟจาโบทินสกี (Belousov Zhabotinsky reaction) ซึ่งเป็นเสมือนแบบจำลองสำหรับการศึกษาพลศาสตร์ของขดคลื่นลายก้นหอยในระบบต่างๆ ทั้งนี้เพราะพลศาสตร์ของระบบเหล่านี้มีลักษณะที่คล้ายคลึงกัน ดังนั้นความเข้าใจพลศาสตร์ของขดคลื่นในระบบๆหนึ่ง จึงนำไปสู่การเข้าใจพลศาสตร์ของขดคลื่นในระบบอื่นๆด้วย อีกทั้งปฏิกิริยาเบลูซอฟจาโบทินสกีเป็นระบบเชิงเคมีที่สามารถควบคุมตัวแปรต่างๆและทำซ้ำได้ง่ายสำหรับการทดลองในห้องปฏิบัติการ

จากการศึกษาการควบคุมพลศาสตร์ของขดคลื่นในปฏิกิริยาเบลูซอฟจาโบทินสกีจะนำไปสู่การเข้าใจพลศาสตร์ของขดคลื่นได้อย่างลึกซึ้งมากขึ้น ไปจนถึงสามารถนำความรู้หรือแนวคิดที่ได้จากการควบคุมขดคลื่นนี้ ไปใช้ประโยชน์ในการควบคุมขดคลื่นในระบบอื่น ๆ ที่มีความซับซ้อนแต่มีพฤติกรรมคล้ายคลึงกับพฤติกรรมของปฏิกิริยาเบลูซอฟจาโบทินสกีได้ เช่น ขดคลื่นที่เกิดจากการหดตัวของกล้ามเนื้อหัวใจในภาวะที่การเต้นของหัวใจล้มเหลว เป็นต้น

2. วัตถุประสงค์

งานวิจัยนี้มีวัตถุประสงค์เพื่อศึกษาและพัฒนาการควบคุมพลศาสตร์ของขดคลื่นในปฏิกิริยาเบลูซอฟจาโบทินสกีที่ไวแสง ในอันที่จะเข้าใจธรรมชาติและพลศาสตร์ของขดคลื่นในระบบต่างๆให้ลึกซึ้งมากยิ่งขึ้น

3. ระเบียบวิธีการวิจัย

การควบคุมขดคลื่นทำได้โดยการฉายแสงเป็นช่วงสั้นๆ (light pulse) ในขณะที่คลื่นเคลื่อนที่ผ่านจุดที่เรียกว่าจุดวัด (measuring point) ที่กำหนดไว้ หรือรอด้วยความหน่วงเวลา (time delay) คงที่ค่าหนึ่ง การควบคุมแบบป้อนกลับนี้ทำให้มีการเลื่อน (drift) ของแกนของขดคลื่น (spiral wave core) เป็นวงโคจร ที่เรียกว่าเรโซแนนซ์แอตแทรกเตอร์ (resonance attractor) โดยที่วงโคจรนี้มีรัศมีที่ต่างกันเป็นชุดๆซึ่งสอดคล้องกับผลการศึกษาในเชิงคำนวณ (numerical analysis) นอกจากนี้การเปลี่ยนค่าตัวแปรของการควบคุมแบบป้อนกลับส่งผลให้เกิดการข้าม ระหว่างวงโคจร ดังนั้นจึงนำไปสู่การควบคุมการเลื่อน (drift) ของแกนของขดคลื่น (spiral wave core) แบบก้นหอย (snail-shaped) ซึ่งมีระยะระหว่างจุดวัด (measuring point) และแกนของขดคลื่น (spiral wave core) เพิ่มขึ้นเรื่อยๆเป็นลำดับ

เมื่อการหน่วงเวลา (time delay) ในวงจรการควบคุมแบบป้อนกลับมีค่ามากกว่าคาบของการหมุน ทำให้เสถียรภาพ (stability) ของเรโซแนนซ์แอตแทรกเตอร์ (resonance attractor) สูญเสียไป โดยเกิดการบิดเบี้ยว (deviation) ไปของวงโคจรรูปวงกลมเดิม ทฤษฎีซึ่งอธิบายพลศาสตร์ของขดคลื่นโดยการส่งแบบวนซ้ำอันดับสูงขึ้นไป (higher order iterative map) ชี้ให้เห็นว่า การสูญเสียเสถียรภาพของเรโซแนนซ์แอตแทรกเตอร์ เป็นผลเนื่องมาจากไนมาร์กไบเฟอร์เคชัน (Neimark bifurcation) ของการส่งแบบ (map)

การควบคุมแบบป้อนกลับอีกชนิดหนึ่งเรียกว่า การควบคุมป้อนกลับแบบครอบคลุม (global feedback) ซึ่งสัญญาณของการควบคุมนั้นคำนวณมาจากพื้นที่รูปวงกลมของปฏิกิริยา (integration area) แสดงให้เห็นถึงการมีเสถียรภาพและการไร้เสถียรภาพของขดคลื่น รวมทั้งการมีแอตแทรกเตอร์ (attractor) ชนิดใหม่เกิดขึ้น ผลการทดลองที่สังเกตได้บางส่วน สามารถอธิบายได้ด้วยคำอธิบายทางคณิตศาสตร์ที่พัฒนาขึ้น โดยเฉพาะการควบคุมแบบหลังสุดนี้ยังมีประเด็นที่น่าสนใจหลายประเด็นที่ควรจะศึกษาและค้นคว้าต่อไป อาทิเช่น การเปลี่ยนขนาดและรูปร่างของ integration area จากวงกลมเป็นสามเหลี่ยม สี่เหลี่ยม และรูปหลายเหลี่ยมอื่นๆ

4. การดำเนินการวิจัยตลอดโครงการในแต่ละช่วง 6 เดือน

ระยะเวลา	แผนการดำเนินการวิจัย
ก.ค. 46 – ธ.ค. 46	- เตรียมปฏิกิริยาเบลูซอฟจาโบทินสกี - เตรียมอุปกรณ์และเครื่องมือในการจับภาพการเคลื่อนที่ของขดคลื่นทำการทดลอง - เขียนโปรแกรมคอมพิวเตอร์ที่ใช้ในการควบคุมแบบป้อนกลับ
ม.ค. 47 – มิ.ย. 47	- ทำการทดลอง โดยใช้การควบคุมแบบป้อนกลับชนิดครอบคลุม โดยเปลี่ยนตัวแปรของการควบคุมชนิดต่างๆ เช่น รูปร่างและขนาดของพื้นที่ของการควบคุม - ทำ numerical simulation ที่สอดคล้องกับการทดลองในห้องปฏิบัติการข้างต้น
ก.ค. 47 – ธ.ค. 47	- ทำการทดลอง โดยใช้การควบคุมแบบป้อนกลับชนิดอื่นๆ เช่น การควบคุมแบบป้อนกลับแบบเฉพาะที่ - ทำ numerical simulation ที่สอดคล้องกับการทดลองในห้องปฏิบัติการข้างต้น
ม.ค. 48 – มิ.ย. 48	- วิเคราะห์และเปรียบเทียบผลการทดการทดลองกับ numerical simulation - อธิบายพลศาสตร์ที่สังเกตได้ในเชิงทฤษฎี

5. ผลงาน/หัวข้อเรื่องที่ตีพิมพ์ในวารสารวิชาการระดับนานาชาติในแต่ละปี

5.1 Kheowan, O., Kantrasiri S., Uthaisar C., Gáspár V., and Müller, S.C., "Spiral Wave Dynamics Controlled by a Square-Shaped Sensory Domain", *Chem. Phys. Lett.* **389** (2004) 140. (impact factor: 2.438)

5.2 Kheowan, O., Kantrasiri S., Wilairat P., Storb U., and Müller, S.C., "Spiral wave dynamics under feedback control derived from a variety of sensory domains", *Phys. Rev.* E **70** (2004) 46221-46225. (impact factor: 2.202)

5.3 Kheowan, O., Uthaisar C., Kantrasiri S., and Müller, S.C., "Hypocycloidal resonance attractor for rigidly rotating spiral waves", *Chem. Phys. Lett.* **399** (2004) 506-511. (impact factor: 2.438)

6. งบประมาณโครงการ (ตามระยะเวลาโครงการที่ได้เสนอรับทุน)

	ปีที่ 1	ปีที่ 2	รวม
1. หมวดค่าตอบแทน - ค่าตอบแทนหัวหน้าโครงการ	120,000	120,000	240,000
2. หมวดค่าวัสดุ - ค่าสารเคมี - ค่าเครื่องแก้วและวัสดุอื่นๆ	70,000 47,000	70,000 47,000	140,000 94,000
3. หมวดค่าใช้สอย	3,000	3,000	6,000
รวมงบประมาณโครงการ	120,000	120,000	240,000

เนื้อหางานวิจัย

I. Spiral wave dynamics controlled by a square-shaped sensory domain

Introduction

Controlling the dynamics of spiral waves is important for many excitable media including chemical systems like the CO oxidation on platinum surfaces [1], the Belousov-Zhabotinsky (BZ) reaction [2, 3] or biological systems like neuronal [4] or cardiac tissue [5, 6]. Effective control methods include external (periodic) forcing [7, 8, 9] or more complex feedback algorithms [10] that are based on collecting data on the activity level of the system and transforming this information to a spatially uniform modulation of the excitability of the medium. The activity level can be measured at one point (local feedback) [9, 11], in a given domain (nonlocal feedback) [12, 13] and at all points (global feedback) [14]. Of both theoretical and practical interest is the effect of shape and size of the applied "sensory domain" on the dynamics of rotating spiral waves under feedback control. Here we apply square-shaped domains and find a broad spectrum of dynamical responses, including square-shaped and cross-shaped trajectories. Numerical simulations using the light-sensitive Oregonator model [15, 16] reproduce this behaviour. We suggest that the feedback method introduced in this work offers an efficient tool for controlling also the dynamics of other excitable media.

Experimental method and results

We study spiral wave dynamics in thin layers of the BZ reaction with the light-sensitive $Ru(bpy)_3^{2+}$ catalyst [17, 18]. This catalyst promotes the autocatalytic production of $HBrO_2$, the activator species of the BZ system. The applied illumination enhances the production of the bromide ion, an inhibitor species, and thus decreases the system's excitability which, in turn, results in slowing down the wave activity in the medium. This provides an experimentally accessible method to control spiral wave dynamics [18], in that the light intensity influences parameters such as the wavelength and the diameter of the spiral core.

In our experiments, the $Ru(bpy)_3^{2+}$ catalyst was immobilized in a silica gel matrix [19] (thickness 0.3 mm, diameter 5 cm) at a concentration of 4.2 mM. The reactants and their concentrations (disregarding bromination of malonic acid) were: $NaBrO_3$ (0.20 M), malonic acid (0.17 M), H_2SO_4 (0.39 M) and NaBr (0.09 M) [17, 18]. The experiments were carried out at an ambient temperature of $25 \pm 1°C$. We created a spiral wave by using a spot (diameter, 1 cm) of intense light from a cold light source to break a propagating wave front (this creates two wave ends) and suppressing one of the open ends with the light spot to leave a single spiral in the center of the dish [11]. The reaction layer was uniformly illuminated from below with a video projector controlled by a computer via a frame grabber. The oxidation waves were observed in transmitted light by a CCD camera and stored on a computer. The main features of spiral rotation, the trajectory of spiral tip, is determined by a special computer procedure given in ref. 9.

In our non-local feedback algorithm, the illumination intensity applied to the reaction layer is given by [12]

$$I(t) = I_0 + k_{fb}[B(t) - B_0], \qquad (1)$$

where I_0 is a constant background intensity. $B(t)$ is the average grey level of the pixels in the square-shaped sensory domain:

$$B(t) = \frac{1}{n} \sum_{i=1}^{n} G_i(t), \qquad (2)$$

where $0 \leq G_i \leq 255$ is the grey level of a given pixel, and n is the total number of pixels in the domain. Note that a larger grey level corresponds to higher concentration of the oxidized form of the catalyst (bright fronts). The intensity of the feedback illumination $I(t)$ is controlled by the gain k_{fb}, and the value of $B(t)$. The constant B_0 is the $B(t)$ averaged over one period of a spiral placed in the center of the square domain and illuminated with background intensity I_0.

The effects of such nonlocal feedback on a rigidly rotating spiral wave are shown in Fig. 1. For a side length d of the domain significantly smaller than the spiral wavelength λ ($d = 0.5\lambda$), the spiral leaves the center of the sensory domain, where its circular core was initially placed [arrow in Fig. 1(a)], by drifting outwards until it makes a turn to follow a circular path with a radius of about 0.76λ. This motion resembles that observed in earlier reported experiments applying a small size, circular-shaped sensory domain [12].

For a domain size equal to the spiral wavelength ($d = \lambda$), the spiral core first drifts away from the domain center [Fig. 1(b)], then it approaches a stable, square-shaped trajectory with a side length of about
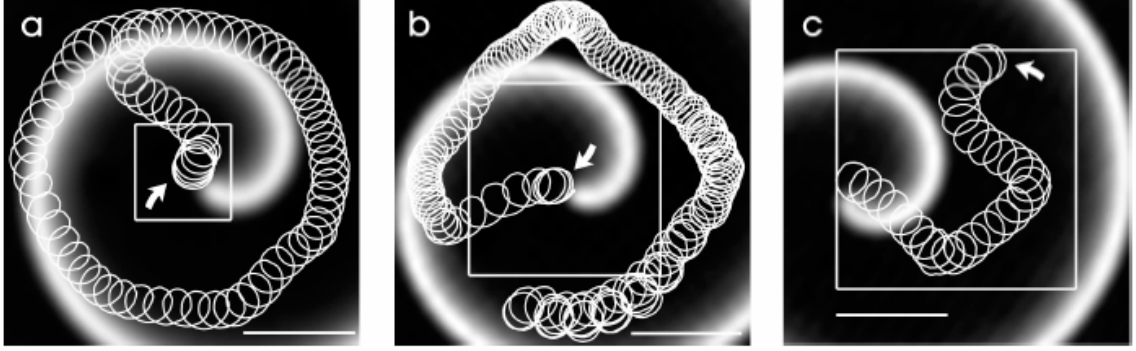
Figure 1: Experimental trajectories of a spiral wave tip subjected to the feedback control Eqs. (1-2) for different sizes of the sensory domain: (a) $d = 0.5\lambda$ (λ = spiral wavelength) with $B_0 = 24$, $k_{fb} = 0.2$, (b) $d = 1.0\lambda$ with $B_0 = 24.5$, $k_{fb} = 0.8$, and (c) $d = 1.25\lambda$ with $B_0 = 19$, $k_{fb} = 0.45$. $I_0 = 0.70\,\mathrm{mW\,cm^2}$ for all experiments. The domains and the initial spiral core locations are indicated by squares and thick arrows, respectively. The spiral images are shown for the start of the trajectory in (a) and (b) and the end of the trajectory in (c). Scale bar: 1 mm.

1.33λ, which is rotated by about 45 degrees with respect to the domain. Note that the drift velocity of the spiral wave core changes periodically: it is slower at the corners and faster at the sides of the trajectory.

Figure 1(c) shows the trajectory of the spiral tip in an experiment with a still larger feedback domain, $d = 1.25\lambda$. In this case, the spiral tip was initially placed close to the domain boundary. The feedback control induces first a drift towards the center and subsequently towards the middle region of the adjacent side of the domain. This process occurs several times and consequently the spiral tip is caught inside the square, bouncing from and to the "virtual walls". Figs. 1(a-c) indicate that increasing the size d of the feedback domain has a pronounced effect on the shape and size of the spiral tip trajectory. In certain ranges of increasing d, the size of the square trajectory is reduced. Experiments also show that the trajectories act like attractors: the spiral tip always approaches them independently from its initial position.

Numerical results and discussion

We complemented the experiments by numerical simulations using the Oregonator model [15, 16], extended by a term $\phi = \phi(t)$ accounting for the effect of bromide ion produced due to the illumination [20]:

$$\frac{\partial u}{\partial t} = \frac{1}{\epsilon}[u - u^2 - (fv + \phi)\frac{u - q}{u + q}] + \nabla^2 u, \tag{3}$$

$$\frac{\partial v}{\partial t} = u - v. \tag{4}$$

Here, the variables u and v describe the evolution of the concentration of the autocatalytic species $HBrO_2$ and the oxidized form of the catalyst, respectively. Due to the immobilization of the catalyst, variable v does not diffuse in this model. The parameters $\varepsilon = 0.05$, $q = 0.002$ and $f = 3.5$ are kept constant. Nonlocal feedback is introduced into the model by varying the value of $\phi(t)$ according to [14]

$$\phi(t) = \phi_0 + k_{fb}[\tilde{B}(t) - \tilde{B}_0], \tag{5}$$

$$\tilde{B}(t) = \frac{1}{S}\int_s v\,ds \tag{6}$$

where ϕ_0 is constant (=0.01). The integral $\tilde{B}(t)$ takes into account the effect of the average wave activity in the square-shaped sensory domain S. The constant $\tilde{B}_0$ refers to this integral averaged over one period of a spiral placed in the domain center with constant production term $\phi(t) = \phi_0$.

Figure 2(a) shows the result of calculations based on Eqs. (3-6) with $d = \lambda$ (41 s.u.) and $k_{fb} = 0.1$. The spiral core was initially located at the center of the sensory domain. Switching on the feedback control induces the drift of the spiral core first outwards from the center and then along a square-shaped trajectory, in good agreement with the experimental results [Fig. 1(b)]. In the parts of the trajectory labeled 1 and 4 the center of the core drifts approximately along a straight line. In part 2 the trajectory starts to bend and to slow down and then turns by 90° in part 3. Corresponding changes in the illumination intensity $\phi(t)$ are shown in Fig 2(b). The feedback algorithm is turned on at $t = 20$ (after about 3 rotations) resulting in
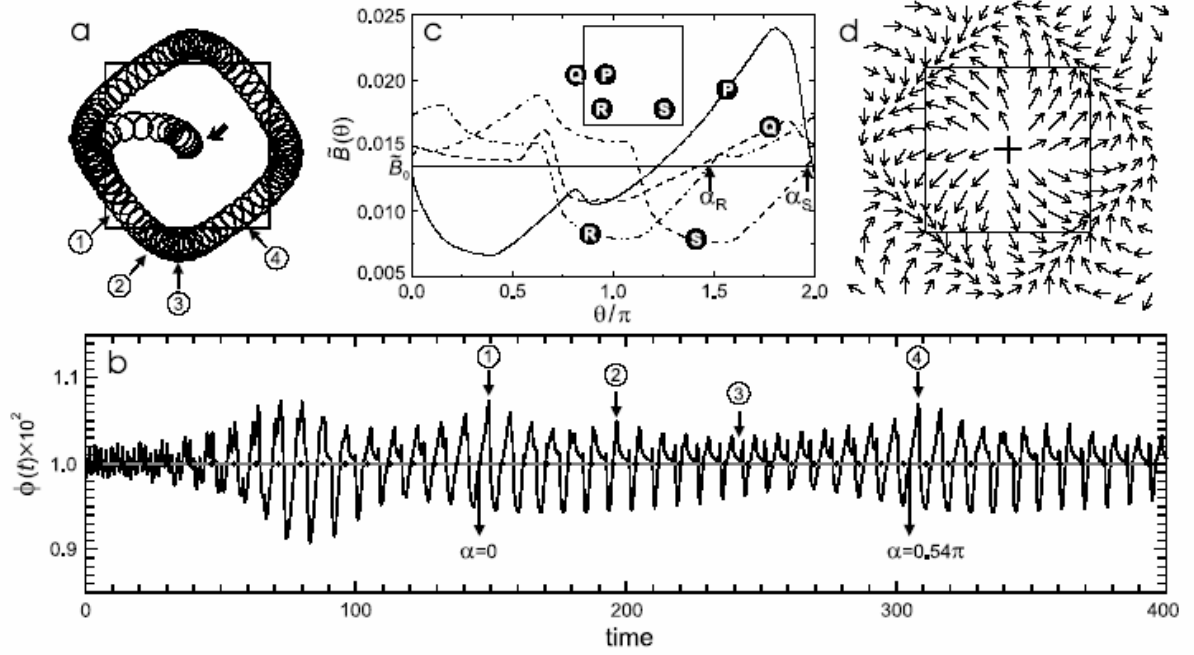
Figure 2: Spiral wave simulated by Eqs. (3-6) under feedback control derived from a square domain with $d = \lambda$. The computations were performed by the explicit Euler method, using a five-point approximation of the Laplacian on a 384×384 array with a grid spacing $\triangle x = 0.5$ and time step $\triangle t = 0.001$. (a) Trajectory of spiral wave tip under a feedback control with $k_{fb} = 0.10$. (b) Value of $\phi(t)$ corresponding to the trajectory in (a). The feedback was switched on at time $= 20$. α is the rotation phase. (c) Analysis of integral [Eq. (6)] as a function of the rotation angle θ of the spiral wave (without feedback) for different locations of the spiral wave core. Each curve is labeled by letters that correspond to those in the square domain (insert) and indicate the location of the spiral core. $\tilde{B}_0$ is the average value of $\tilde{B}(\theta)$ for one rotation of a spiral placed at the domain center. Rotation phases given by arrows are: $\alpha_R = 1.48$, $\alpha_S = 1.97$. (d) Flow map of spiral core trajectory. Arrows indicate the velocity and the direction of the drift. Distance between data points is $1/8\lambda$. The direction of each vector is determined from the difference between the phase of $\tilde{B}$ at that point (arrow tail) and a reference phase (in this case $\pi/4$). Its modulus is calculated as the integral of $|\tilde{B}(\theta) - \tilde{B}_0|$ over one period of the rotation angle θ.

large amplitude oscillations of the ϕ values. To show a slight shift in the phase of this oscillation, black dots have been plotted on the abscissa at an interval equal to the oscillation period measured at the part of the trajectory labeled 1. Using these 'stroboscopic' dots, the phase shift, for example, between points labeled 1 and 4 can be determined as 0.54π, which agrees well with the angle difference of the drift directions (90°) at points 1 and 4 of the square-shaped trajectory in Fig 2(a).

The oscillations in $\phi(t)$ are due to corresponding changes of the value of the integral in Eq. (6), which we analyze by considering unperturbed spirals (without feedback) placed inside and outside the quadratic sensory domain. The location of the spiral tip is indicated by black circles labeled with letters P-S, as indicated in the quadratic insert of Fig. 2(c). These black circles depict the locations of the spiral core along the trajectory in Fig. 2(a). For example, points R and S in the insert correspond to the parts of the trajectory in Fig. 2(a), labeled 1 and 4, respectively.

The $\tilde{B}$-values are calculated and plotted in Fig. 2(c) for one rotation of the spiral ($0 \leq$ rotation angle $\theta \leq 2\pi$), without feedback. Here, $\tilde{B}$ can be written as a function of the rotation angle $\theta(t)$, which is proportional to time t, i. e. $\tilde{B} = \tilde{B}(\theta)$. The horizontal line in this graph corresponds to $\tilde{B}_0$, as specified in the caption. Curves $\tilde{B}(\theta)$ oscillate with different shape and amplitude for different locations P-S. Considering the extrema of these curves $\tilde{B}(\theta)$, their high values at location P result in a large perturbation and therefore a fast drift of the spiral wave core, as observed in Fig. 2(a). Around location Q, corresponding to one of the corners of the square-shaped trajectory in Fig. 2(a), the values of these extrema drop, therefore the drift around the corners is slow. In order to explain the direction of the drift, the phase of curve $\tilde{B}(\theta)$ must be characterized. Note that all shown curves cross the reference line, $\tilde{B}(\theta) = \tilde{B}_0$, with a positive
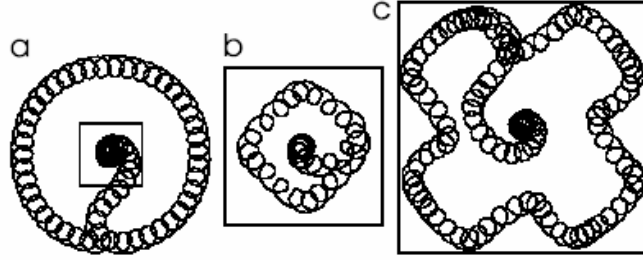
3

Figure 3: Simulation results of the spiral wave dynamics under a feedback control derived from different sizes of the domain (a) $d = 0.5\lambda$, $k_{fb} = 0.10$, (b) $d = 1.25\lambda$, $k_{fb} = 0.20$, and (c) $d = 2\lambda$, $k_{fb} = 0.50$. Trajectories (a) and (b) correspond to experiments shown in Figs. 1(a) and (c), respectively.

slope only once during a rotation period. In order to further characterize these curves, the value of the rotation angle at the intersections is defined as the rotation phase α. One can see that the shapes of the $\tilde{B}(\theta)$ curves at locations R and S (with drift directions that are perpendicular to each other) are similar, but their phases differ by about 0.5π [compare α_R and α_S in Fig. 2(c)]. This corresponds well to the phase shift of 0.54π in the feedback signal in parts 1 and 4 of Fig. 2(b).

For a more detailed analysis, the local values of $\tilde{B}(\theta) = \tilde{B}_{x,y}(\theta)$ were determined on a finer grid of core locations (x,y). This provides the possibility to construct a flow map shown in Fig. 2(d). As described in the caption, this flow map is based on phases representing the drift directions. The integral of $|\tilde{B}(\theta) - \tilde{B}_0|$ over one period is taken as a measure for the magnitude of the perturbation and represents the drift velocity. Most of the flow vectors are attracted towards a square trajectory, on which they are caught in a counterclockwise motion, in agreement with the observed attractor in Fig. 2(a).

The dynamics of such an attractor changes with the size of the integration domain. For a rather small domain ($d = 0.5\lambda$) one obtains a circular attractor [Fig. 3(a)], similar to that of Fig. 1(a). Here, the four-fold geometry of the sensory domain is not reflected in the shape of the trajectory. For domains larger than the spiral wavelength, the size of the attractor decreases, as shown in Fig. 3(b) where $d = 1.25\lambda$. The 90 degree turns of the drift direction close to the virtual walls agree with the experimental observation [Fig. 1(b)]. An interesting cross-shaped trajectory is created by further increasing the domain [Fig. 3(c)].

Our experimental and numerical results demonstrate that the considered nonlocal feedback algorithm is highly efficient to control spiral wave dynamics. The method can be easily transferred to control the dynamics of spatially extended systems of other types, e.g. in biology [4, 5]. The size and shape of a sensor by which we collect information about the activity level of a dynamical system turns out to be crucial and decisive on determining the size and shape of the spatiotemporal attractor governing the behaviour of the system under feedback control.

References

[1] S. Jakubith, H.H. Rotermund, W. Engel, A. von Oertzen, and G. Ertl, *Phys. Rev. Lett.* **65** (1990) 3013.

[2] A.T. Winfree, *Science* **175** (1972) 634.

[3] S.C. Müller, T. Plesser, and B. Hess, *Science* **230** (1985) 661.

[4] N.A. Gorelova and J. Bureš, *J. Neurobiology* **14** (1983) 353.

[5] J.M. Davidenko, A.V. Pertsov, R. Salomonsz, W. Baxter, and J. Jalife, *Nature*(London) **355** (1992) 349.

[6] A.T. Winfree, *When time breaks down* (Princeton University Press, Princeton, 1987).

[7] K.I. Agladze, V.A. Davydov, and A.S. Mikhailov, *JETP Lett.* **45** (1987) 767.

[8] O. Steinbock, V.S. Zykov, and S.C. Müller, *Nature* **366** (1993) 322.

[9] S. Grill, V.S. Zykov, and S.C. Müller, *Phys. Rev. Lett.* **75** (1995) 3368.

[10] T. Sakurai, E. Mihaliuk, F. Chirila, and K. Showalter, *Science* **296** (2002) 2009.

[11] O. Kheowan, V.S. Zykov, O. Rangsiman, and S.C. Müller, *Phys. Rev. Lett.* **86** (2001) 2170.

[12] O. Kheowan, C.K. Chan, V.S. Zykov, O. Rangsiman, and S.C. Müller, *Phys. Rev. E* **64** (2001) 35201.

[13] V.S. Zykov, G. Bordiougov, H. Brandtstädter, I. Gerdes, and H. Engel, *Phys. Rev. Lett.* **92** (2004) 18304.

[14] V.S. Zykov, A.S. Mikhailov, and S.C. Müller, *Phys. Rev. Lett.* **78** (1997) 3398.

[15] R.J. Field and R.M. Noyes, *J. Chem. Phys.* **60** (1974) 1877.

[16] W. Jahnke and A.T. Winfree, *J. Bifur. and Chaos* **1** (1991) 445.

[17] V. Gáspár, Gy. Bazsa, and M.T. Beck, *Z. Phys. Chem.* (Leipzig) **264** (1983) 43.

[18] L. Kuhnert, *Naturwissenschaften* **73** (1986) 96.

[19] T. Yamaguchi, L. Kuhnert, Zs. Nagy-Ungvarai, S.C. Müller, and B. Hess, *J. Phys. Chem.* **95** (1991) 5831.

[20] H.J. Krug, L. Pohlmann, and L. Kuhnert, *J. Phys. Chem.* **94** (1990) 4862.

II. Spiral wave dynamics under feedback control derived from a variety of sensory domains

Introduction

The implementation of control strategies to manipulate complex oscillations and spatiotemporal patterns has become a central issue of nonlinear dynamics. Feedback methods provide one of the possible control techniques that yield new modes of spatiotemporal behaviour [1, 2]. These techniques may be designed in different ways. A feedback is global or nonlocal, in contrast to local techniques, if the control signal represents a sum of contributions from all or many parts of the system. Such feedbacks have been used, for instance, to control spatiotemporal activity in the Pt-catalyzed oxidation of CO [3], suggesting a means for enhancing catalytic efficiency [4]; in gas discharges to suppress plasma instabilities [5]; in electrochemical systems to influence spatial coupling among different active sites [6]; and in semiconductors in connection with charge transport phenomena [7]. Propagating waves [8] and, in particular, spiral waves [9, 10, 11, 12] in the Belousov-Zhabotinsky (BZ) reaction [13, 14] have also been controlled by using these feedback methods, which points to the possibility of manipulating dynamical patterns in excitable media including excitable biological tissues [15, 16, 17]. A recent advance in this direction is the control of seizure-like events in hippocampal brain slices with adaptive electric fields [18]. Thus, the ability to regulate spatiotemporal behaviour provides both a means of generating desired dynamical patterns and the tools for probing underlying mechanisms.

In this work we perform a numerical study of rigidly rotating spiral waves subjected to a nonlocal feedback derived from a confined "sensory domain". A time-dependent spatially uniform modulation of the system's excitability is taken to be proportional to the integral light absorption observed within this domain. Of both theoretical and practical interest are the geometrical features of the applied sensory domain on the dynamics of the rotating spirals [9, 10, 11, 12, 13]. We apply the feedback with different shapes and sizes of the domain and find a broad spectrum of dynamical responses, including various shapes of the spiral tip trajectories and the switching between their stability properties. A flow map and a bifurcation diagram are constructed in order to analyze the observed phenomena.

Simulation method

Our computations are performed with the light-sensitive two-variable Oregonator model [19, 20, 21], which has been successfully used to describe the dynamics of the photosensitive BZ system by including a flux term $\phi = \phi(t)$ for the light-induced bromide production [21]:

$$\frac{\partial u}{\partial t} = D_u \nabla^2 u + \frac{1}{\epsilon}[u - u^2 - (fv + \phi)\frac{(u-q)}{(u+q)}], \tag{1}$$

$$\frac{\partial v}{\partial t} = u - v. \tag{2}$$

Here, the variables u and v describe the evolution of the concentration of the autocatalytic species $HBrO_2$ and the oxidized form of the catalyst, respectively. $D_u = 1$ is the scaled diffusion coefficient of variable u. The catalyst is assumed to be immobilized in a gel matrix, thus variable v does not diffuse in this model ($D_v = 0$). The parameters have the values $\epsilon = 0.05$, $q = 0.002$, and $f = 3.5$, which are kept constant. The computations were performed by an explicit Euler method, using the five-point approximation of the Laplacian on a 384×384 array with a grid spacing $\triangle h = 0.5$ s.u. and time step $\triangle t = 0.001$ t.u.

The feedback signal is determined by the integral of wave activity taken over the sensory domains, expressed as [22]

$$\phi(t) = \phi_0 + k_{fb}[\widetilde{B}(t) - \widetilde{B}_0] \tag{3}$$

with

$$\widetilde{B} = \int_S u dS, \tag{4}$$

where ϕ_0 is constant (=0.01). Thus, the intensity of the feedback signal is controlled by the coefficient k_{fb} and depends linearly on the integral value $\widetilde{B}$ of the variable u over the domain S. The constant $\widetilde{B}_0$ refers to this integral averaged over one period of a spiral placed in the domain center with constant flux term $\phi(t) = \phi_0$.
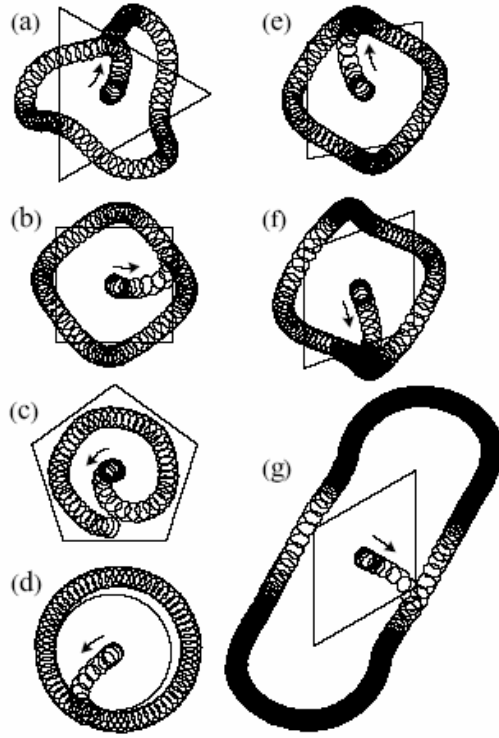
Results

Figure 1: Trajectories of the spiral wave tip derived from simulations for different shapes of the sensory domain starting from an initial location of the spiral core at the domain center. (a) Triangle, side length 1.50λ, $k_{fb} = 0.05$; (b) square, side length 1.00λ, $k_{fb} = 0.11$; (c) pentagon, side length 0.75λ, $k_{fb} = 0.15$; (d) circle, diameter 1.00λ, $k_{fb} = 0.08$; (e-g) rhombus, side length 1.00λ and $k_{fb} = 0.10$; acute angles: $80°$, $70°$ and $60°$, resp. The feedback mechanism is computed from Eqs. (3)-(4). Arrows indicate drift direction of the spiral core.

A single spiral is induced from the equation system (1)-(2) by choosing a special initial condition [23]. The variables u and v are initially set to zero uniformly in the medium. To create a spiral then we introduce a nonuniform distribution of the variables. A super-threshold value $u = 1$ is given along a line near the boundary of the excitable medium to induce a propagating wave. After this wave has reached the center of the excitable medium, one half of the planar wave is erased by resetting $u = v = 0$. Subsequently, the open end of the planar wave curls into a spiral wave with its core located near the center of the excitable medium. Without external forcing and with the above chosen parameter values, the spiral wave rotates rigidly around a circular core with a rotation period $T_0 = 8.2$ t.u. and a wavelength $\lambda = 4.1$ s.u. There is ample evidence [9, 10, 11, 22] that for this kind of nonlocal feedback a spiral wave core placed initially at the center of the sensory domain is destabilized for the case of a positive coupling constant k_{fb} and starts to drift away from the center, as shown in all of the examples of Fig. 1. A previous systematic study of circular sensory domains has shown that it frequently moves asymptotically on a circular attractor [9].

In our simulations we find, how the shape of this type of spiral tip trajectories is transformed when the shape of the sensory domain is varied. For a triangular domain the feedback induces the spiral core to drift away from the domain center and to make a turn on each side with an overall $120°$ change of the drift direction. Finally it describes a trajectory with an approximately threefold symmetry [Fig. 1(a)]. An increase of the number of corners of the sensory domain results in an increase of the number of turning points of the drift direction, as shown in Figs. 1(b)-1(c). For a square-shaped domain [Fig. 1(b)], the trajectory describes a square-shaped pathway, which is rotated by about 45 degrees with respect to the domain. A further increase in the number of domain corners to form a pentagon [Fig. 1(c)] produces a trajectory that follows an approximately pentagonal pathway inside the domain. It appears to be almost circular, because the five rounded corners of the domain are only faintly reflected. For perfect symmetry, as for the circular domain in Fig. 1(d), the trajectory describes a circular pathway around the domain.

Exerting some shear on the square-shaped domain causes a transformation of the trajectory from a square to a rhombic pathway, as shown in Figs. 1(e) and 1(f). A further decrease of the acute angle of the rhombus induces the trajectory to form a large oblong excursion around the domain [Fig. 1(g)]. Now
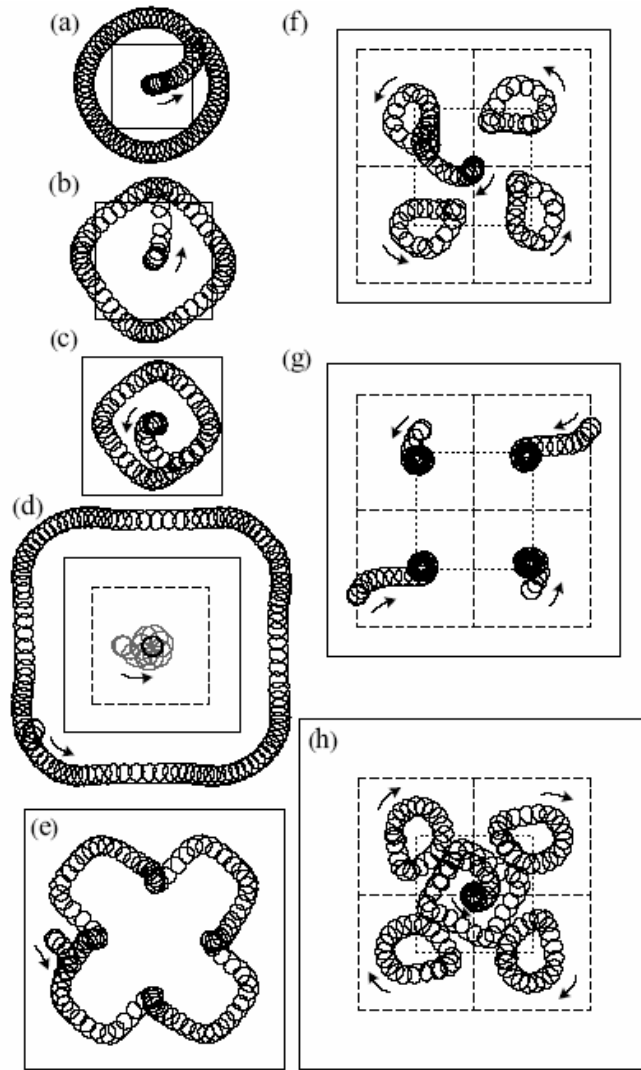
2

Figure 2: Trajectories of spiral wave tip under variation of the size of the square domain. (a-h) Side length $d_s = 0.70\lambda$, 1.00λ, 1.25λ, 1.50λ, 2.25λ, 2.40λ, 2.50λ, 3.00λ; $k_{fb} = 0.05$, 0.15, 0.12, 0.20, 0.40, 0.50, 0.50, 0.75. Arrows indicate the drift direction of the spiral core. The dashed squares with $d_s = \lambda$ indicate the approximate location of the separatrix of basins of attraction, whereas the dotted squares depict a reference domain ($d_s = \lambda$). The gray curve in (d) shows the transient trajectory, before a circular, stable rotation is achieved at the center (black circle).

the drift velocity of the spiral wave core changes drastically along the oblong pathway. It becomes very slow when the spiral wave core is far away from the center of the rhombic domain. The results demonstrate that the shape of the sensory domain is reflected in the dynamics of the spiral tip trajectory.

Besides the shape of the domain it is also its size that plays a crucial role for the spiral dynamics, as shown in Fig. 2. We use the square-shaped domain with side length d_s to study this effect. For a rather small size ($d_s = 0.7\lambda$) one obtains a circular attractor [Fig. 2(a)], not reflecting the fourfold symmetry of the sensory domain. The circular trajectory transforms to a square for $d_s = 1.0\lambda$ [Fig. 2(b)], similar to the one in Fig. 1(b). For domains larger than the spiral wavelength the size of the attractor decreases, as shown in Fig. 2(c) where $d = 1.25\lambda$.

Note that the drift velocity in Fig. 2(b) is larger than that in Fig. 1(b). This increase is connected with the choice of a larger feedback coupling strength. In fact, we found that for fixed size and shape of the sensory domain larger k_{fb} values lead to a faster drift, as long as the shape of the tip trajectory is rather simple as, for instance, for the case of square domains with size $d_s < 1.5\lambda$. For larger d_s the tip dynamics becomes complex (see below) and the influence of k_{fb} cannot be easily predicted.

Two trajectories are observed for $d_s = 1.50\lambda$ [Fig. 2(d)]. A small, flower-like trajectory occurs at the center of the domain, when the unperturbed spiral core is initially placed close to the domain center. Note that the gray curve in Fig. 2(d) represents the transient trajectory before a circular, stable rotation
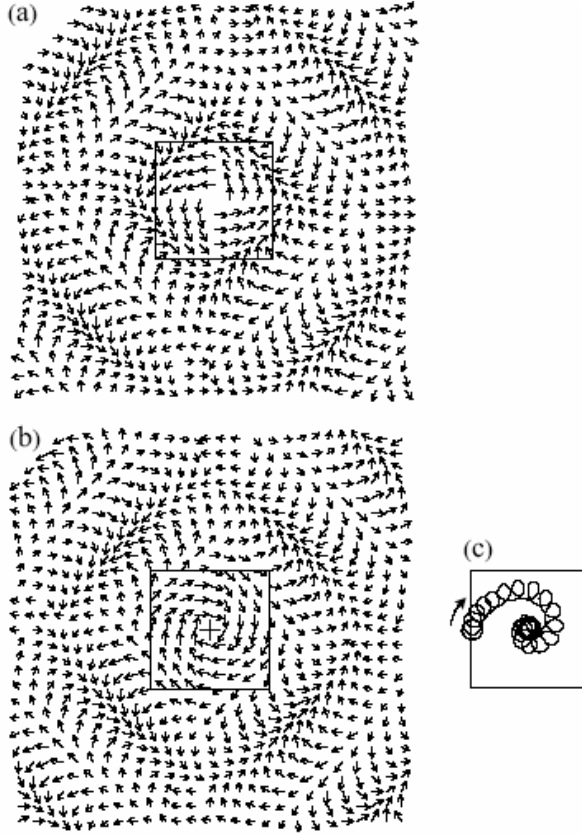
3

Figure 3: (a,b) Vector field plots of the trajectories of the spiral core center under feedback control derived from a square domain with $d_s = \lambda$ for positive feedback (a), and negative feedback (b). (c) Trajectory of the spiral wave tip under negative feedback control with feedback parameters $d_s = 1\lambda$ and $k_{fb} = -0.15$. The arrow indicates the drift direction of the spiral core. Note that the coefficient k_{fb} is not involved in the construction of the vectors in the flow map.

(black circle) is achieved at the center. For a larger initial distance to the domain center, the spiral core is attracted towards a trajectory describing a large square with rounded corners. Its orientation coincides with that of the domain, in contrast to the trajectories in Figs. 2(b) and 2(c), which are rotated by about 45 degrees with respect to the domain. The dashed square with side length λ in Fig. 2(d) indicates the approximate location of the separatrix between two basins of attraction that exist for the motion of the spiral core center. However, the attractor, which is eventually reached, is determined not only by the initial location of the spiral core but also by the initial location of the tip with respect to the core center (the initial phase). Thus the location of the separatrix depends on this initial phase, which slightly blurs this separating line. We checked numerically that the blurring effect of the initial phase is below 0.024λ.

An interesting cross-shaped trajectory is created when increasing the domain size to $d_s = 2.25\lambda$ [Fig. 2(e)]. This trajectory can be considered as a combination of four small pieces of square-shaped trajectories, which are linked together. With a further increase of d_s to 2.40λ, there appear four trajectories, which are separated from each other [Fig. 2(f)]. Note that the shape of the trajectories changes from a square- to a drop-like form. Which of these four possible stable orbits is reached depends now on the initial location of the unperturbed spiral core center. The approximate separatrices between the basins of attraction of each orbit are shown by dashed boxes [Fig. 2(f)].

The dynamics of the four attractors in Fig. 2(f) can be stabilized by enlarging the domain to $d_s = 2.50\lambda$ [Fig. 2(g)], the unperturbed spiral wave core is placed at four different locations inside the domain. The feedback induces the spiral wave core to drift towards four stable points (indicated by arrows), located approximately at the corners of the reference domain $d_s = \lambda$ [dotted square in Fig. 2(g)]. At these points, the spiral rotates rigidly without drift. When the domain size is further increased to $d_s = 3.00\lambda$, the locations of these four points become again unstable [Fig. 2(h)], i.e., the spiral wave drifts again along a drop-like pathway. Note that the drift direction of these drop-like attractors is clockwise and the petals of the loopy trajectories are directed outwards, in contrast to those in Fig. 2(f). In addition, a new square-shaped trajectory with inward directed petals appears around the center of the domain.
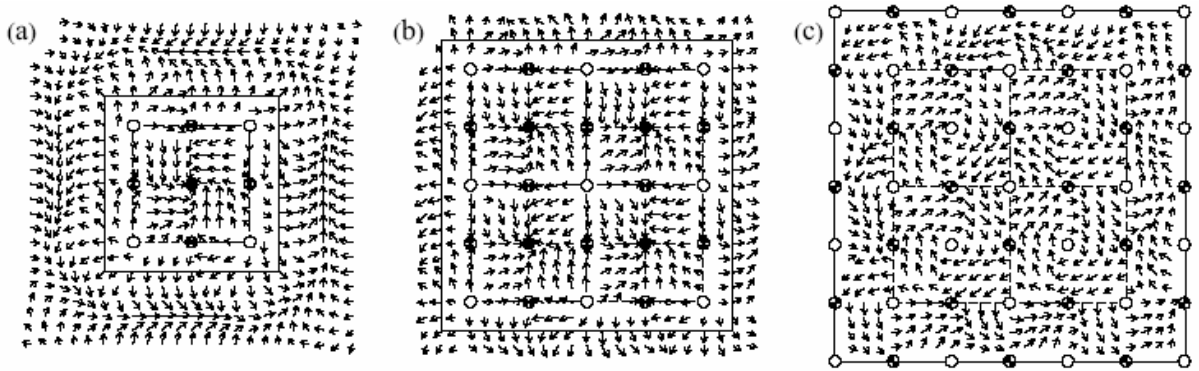
4

Figure 4: Flow maps of the spiral core center under variation of the domain sizes for positive feedback, for (a) $d_s = 1.50\lambda$, (b) $d_s = 2.50\lambda$, and (c) $d_s = 3.00\lambda$. Vectors show the drift direction of the spiral core center, which its size indicates the drift velocity. The dashed line indicates the location of the separatrix, that restricts the basin of each attractor. Closed, open, and checked circles indicate the fixed points: stable node, unstable node and saddle point, respectively.

The dynamics of the trajectories in Fig. 2 can be divided into two types: stable and unstable spiral rotation. Stable rotation means that the spiral rotates rigidly without drift, as illustrated by the trajectories in Fig. 2(d) (small attractor at the center) and 2(g). All other trajectories in Fig. 2, for which the motion of spiral waves is accompanied by a drift of the spiral wave core, are considered as an unstable rotation. These results demonstrate that enlarging the domain size leads to a series of switches from unstable to stable spiral rotation and vice versa.

Discussion

Our discussion is based on the analysis of the integral $\widetilde{B}$ [Eq. (4)] as a function of the rotation angle of spirals placed at different locations inside or outside the square-shaped control domain. It has been shown that the phase of the signal $\widetilde{B}$, which determines the phase of the modulation [Eq. (3)], predominantly affects the drift direction and consequently the shape of the trajectory[12]. The average area under this curve is an appropriate measure for the drift velocity in the range of the sensory domains considered here[12]. The phase relation and the average area form the basis of the flow maps constructed inside and outside the sensory domains as shown, for instance, in Fig. 3 for $d_s = \lambda$. The flow vectors observed for positive feedback [Fig. 3(a)], which corresponds to the simulation results observed for $k_{fb} > 0$ in Figs. 1(b) and 2(b), are attracted towards two square-shaped trajectories (side length about 1λ and 3λ) on which they are caught in a counterclockwise motion. The flow map unravels the existence of a discrete set of stable square-shaped orbits, which appear to be attractors for the spiral core drift. The innermost trajectory corresponds to the attractor presented in Figs. 1(b) or 2(b). For the flow map observed for negative feedback [Fig. 3(b)], which is obtained by considering the signal $\widetilde{B}$ mirrored with respect to the reference line $B = B_0$ corresponding to negative sign of k_{fb} in Eq. (3), most of the flow vectors inside the domain spiral slowly into the domain center to form a stabilized rotation. This stabilization is confirmed by the simulation result for the tip motion in Fig. 3(c). In a certain region outside the domain the vectors flow towards a square-shaped trajectory with a side length of about 2λ. These flow maps illustrate, how the dynamics of the spiral wave can be drastically changed by switching the sign of the feedback gain.

Additional flow maps of the spiral core center under variation of the domain size are shown in Fig. 4. The flow map for the domain with $d_s = 1.50\lambda$ is depicted in Fig. 4(a). Here, most of the vectors are attracted towards two types of stable states: a fixed point at the center and a square-shaped orbit in agreement with the trajectories in Fig. 2(d). The basin of attraction of the two states are separated by the separatrix indicated by the dashed square with side length λ. Closed, open, and checked circles in this figure indicate three types of fixed points: i) the stable node (closed circle), which attracts the vector field from all directions, ii) the unstable node (open circle), which repels the vector field in all directions, and iii) the saddle point, which attracts the vector in one direction but repels it in the direction perpendicular to it. For the flow map in Fig. 4(a) there is one stable node located at the center of the domain. It corresponds to the stabilization of rigid rotation and thus to the small attractor in Fig. 2(d). In addition to the stable node at the center of Fig. 4(a), there appear four unstable nodes at the corners and four saddle points on the edges of the reference domain (dashed square).

The flow map for a larger domain ($d_s = 2.50\lambda$) is shown in Fig. 4(b). It corresponds to the trajectories in Fig. 2(g). The locations of the four stable nodes in this map coincide with those of the
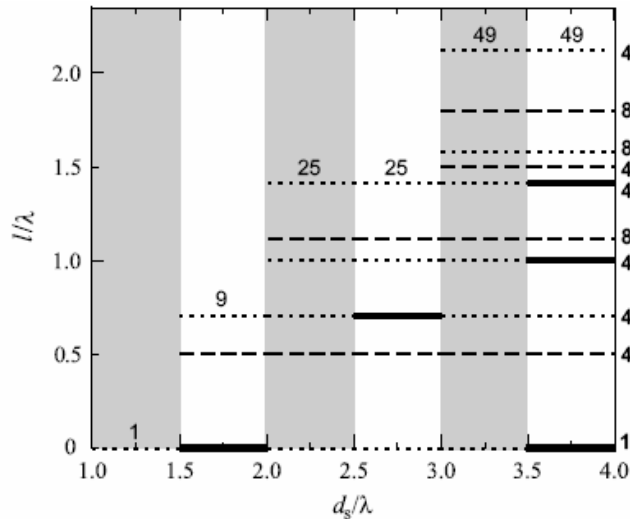
Figure 5: Bifurcation of spiral wave rotation under confined-domain feedback control. Number of fixed points inside the sensory domain is illustrated as a function of the normalized size of the domain, d_s/λ. Location of the fixed point is shown on the y-axis. Solid, dashed and dotted bars indicate the fixed points: stable node, saddle point and unstable node, respectively. Inserted numbers show the total number of fixed points for each range of d_s. Gray bands indicate the range where no stable rotating spirals exist.

unstable ones for $d_s = 1.5\lambda$ [Fig. 4(a)]. Since the distribution of neighboring nodes for each of them is equal to that for the case $d_s = 1.5\lambda$, we find a four-fold symmetric repetition of the pattern of Fig. 4(a). The stability of the four fixed points is lost when enlarging the domain size by about 0.5λ, as shown in Fig. 4(c) for $d_s = 3.0\lambda$. Here, all the fixed points that are stable in Fig. 4(b) become unstable.

The number of fixed points inside the square domain is 9, 25, and 49 for the side lengths $d_s=1.5\lambda$, 2.5λ, and 3.0λ in Figs. 4(a)-4(c), respectively. Note that for domains smaller than 1.5λ, there exists only one unstable fixed point, which is located at the center of the domain, as shown in Figs. 2(a)-2(c) and Fig. 3(a). However, the domain should not be too small, i.e., smaller than the spiral core. Because if such a small domain is located inside the core, there will be no modulation of the signal and consequently no feedback.

The total number of fixed points, F_n, can be described as a function of the the size of the domain d_s according to $F_n = (2n+1)^2$, where $n = [d_s/\lambda - (d_s/\lambda \bmod 1)]$. For example, if $d_s=1.5\lambda$, then $n = 1$ and therefore $F_n = 9$, as shown in Fig. 4(a). Furthermore, the number of each type of fixed point is expressed as i) number of stable nodes, $F_{sn} = n^2$, ii) number of saddle points, $F_{sdn} = 2n(n+1)$, and iii) number of unstable nodes, $F_{un} = (n+1)^2$. One can see clearly that $F_n = F_{sn} + F_{sdn} + F_{un}$. Note that these relationships can be used for $d_s \geq 1.5\lambda$. For $d_s < 1.5\lambda$, $F_n = F_{un} = 1$ as mentioned above.

A bifurcation diagram characterizing the stability of the spiral core drift under a square-domain feedback control is shown in Fig. 5. Stable fixed points exist along the the solid bars in this diagram, whereas the shaded bands indicate the ranges of d_s/λ in which no stable fixed point can be observed. Instead the spiral core moves asymptotically on closed attractive orbits, as previously illustrated for the trajectories evolving from unstable fixed points in Fig. 2 [except for Fig. 2(g) and the small attractor in the middle of Fig. 2(d)]. These properties of these orbits have some analogy to limit cycles in phase space. The number of fixed points increases stepwise with increasing domain size. Focusing on the stable fixed points (solid bars), their number increases as 1, 4, 9,..., corresponding to the relation $F_{sn} = n^2$ mentioned above. In addition, the stability of the fixed points changes also with enlarging the domain. For example, consider the stability of the fixed point located at the center of the domain (distance $l = 0$): the dynamics of this point is unstable for $d_s/\lambda < 1.5$ and becomes stable for $1.5 \leq d_s/\lambda < 2.0$. For $d_s/\lambda \geq 2.0$ it is unstable until $d_s/\lambda \geq 3.5$. Note that the saddle points (dashed bars) keep their characteristics with increasing d_s.

Conclusions

Our results demonstrate that the dynamics of the spiral waves under nonlocal feedback control depends sensitively on the geometry, shape and size of the sensory domain, from which the feedback signal is derived. The results in Fig. 1 show that the geometry of the sensory domain is reflected in the shape of the spiral tip trajectory. For a fixed domain shape, e.g., a square, a small increase of the domain size results

in a decrease of the trajectory size as seen when comparing Fig. 2(b) with 2(c) and Fig. 2(f) with 2(g). Several shapes of the trajectory can be observed by enlarging the domain. Along the axis of increment of the domain size, the dynamics can be divided into two types, stable and unstable rotation, as shown in Figs. 2 and 5.

An explanation of the numerically observed effects is proposed by using flow maps constructed from the analysis of the feedback signal. The flow maps in Fig. 3 reveal that our feedback forcing leads to the existence of a discrete set of stable square-shaped orbits, which appear to be attractors for the spiral core drift. In addition, the flow maps demonstrate that the local and global dynamics of the spiral wave can be drastically changed by switching the sign of the feedback gain [see Figs. 3(a) and 3(b)]. It is shown that the shape and size of the trajectories of the spiral wave tip, as well as the stability of the spiral rotation can be changed by varying the size or shape of the sensory domain. We suggest that the feedback method introduced in this work offers an efficient tool for controlling the dynamics of excitable media in biology [15, 16, 17].

References

[1] H.G. Schuster (ed.), Handbook of Chaos Control (Wiley-VCH, Weinheim, 1999).

[2] E. Ott, C. Grebogi, and J.A. Yorke, Phys. Rev. Lett. **64**, 1196 (1990).

[3] S. Jakubith, H.H. Rotermund, W. Engel, A. von Oertzen, and G. Ertl, Phys. Rev. Lett. **65**, 3013 (1990).

[4] J. Wolff, A.G. Papathanasiou, L.G. Kevrekidis, H.H. Rotermund, and G. Ertl, Science **294**, 134 (2001).

[5] Th. Pierre, G. Bonhomme, and A. Atipo, Phys. Rev. Lett. **76**, 2290 (1996).

[6] K. Krischer, J. Electrochem. **501**, 1 (2001).

[7] G. Franceschini, S. Bose, and E. Schöll, Phys. Rev. E **60**, 5426 (1999).

[8] T. Sakurai, E. Mihaliuk, F. Chirila, and K. Showalter, Science **296**, 2009 (2002).

[9] O.-U. Kheowan, C.K. Chan, V.S. Zykov, O. Rangsiman, and S.C. Müller, Phys. Rev. E **64**, 35201 (2001).

[10] O.-U. Kheowan, V.S. Zykov, and S.C. Müller, Phys. Chem. Chem. Phys. **4**, 1334 (2002).

[11] V.S. Zykov, G. Bordiougov, H. Brandtstädter, I. Gerdes and H. Engel, Phys. Rev. Lett. **92**, 18304 (2004).

[12] O.-U. Kheowan, S. Kantrasiri, C. Uthaisar, V. Gáspár, and S.C. Müller, Chem. Phys. Lett., **389**, 140 (2004).

[13] A.T. Winfree, Science **175**, 634 (1972).

[14] S.C. Müller, T. Plesser, and B. Hess, Science **230**, 661 (1985).

[15] J.M. Davidenko, A.V. Pertsov, R. Salomonsz, W. Baxter, and J. Jalife, Nature (London) **355**, 349 (1992).

[16] M. Dahlem and S.C. Müller, Experimental Brain Research **115**, 319 (1997).

[17] M. Falcke, Y. Li, J.D. Lechleiter, and P. Camacho, Biophys. J. **85**, 1474 (2003).

[18] B.J. Gluckman, H. Nguyen, S.L. Weinstein, and S.J. Schiff, J. Neurobiology **21**, (2001) 590.

[19] R.J. Field and R.M. Noyes, J. Chem. Phys. **60**, 1877 (1974).

[20] W. Jahnke and A.T. Winfree, Int. J. Bifur. and Chaos **1**, 445 (1991).

[21] H.J. Krug, L. Pohlmann, and L. Kuhnert, J. Phys. Chem. **94**, 4862 (1990).

[22] V.S. Zykov, A.S. Mikhailov, and S.C. Müller, Phys. Rev. Lett. **78**, 3398 (1997).

[23] V.S. Zykov and S.C. Müller, Physica D **97**, 322 (1996).

III. Hypocycloidal resonance attractor for rigidly rotating spiral waves

Introduction

Controlling the dynamics of spiral waves is important for many excitable media including chemical systems like the Belousov-Zhabotinsky (BZ) reaction [1, 2, 3, 4, 5, 6], or biological systems like cardiac tissue [7, 8, 9, 10]. One effective control methods is a local feedback algorithm. It has been suggested that this method can be applied to eliminate spiral waves in cardiac tissue [8], i.e., if certain properties of the medium are varied with the period of rotation of a spiral wave, the spiral wave will be subjected to a drift and can be eliminated at the boundary of the medium. Such a local feedback has been realized in the laboratory by disturbing spiral waves in the light-sensitive version of the BZ reaction [11] with a sequence of short light pulses [12, 13, 14, 15, 16, 17, 18]. Each stimulus was applied at an instant corresponding to the passage of the wave front through a particular measuring point. This local feedback mechanism was investigated originally for spirals with a "meandering" tip describing a hypocycloidal trajectory that is characterized by two rotation periods: T_0, as measured at the center of the trajectory and T_∞, as determined far away from it [14].

Under this feedback control two dynamical regimes, called entrainment attractor and resonance attractor, have been observed [14]. The entrainment attractor occurs, if the measuring point is located close to the center of the unperturbed trajectory (initial distance R_0 about 1/3 of the spiral wavelength [14, 15]). The period of external modulation becomes $T_m \approx T_0$, and the tip moves on a hypocycloid in perfect synchrony with the external signal. For larger R_0, the tip is found to move on the resonance attractor. At this larger distance, the average period of the triggered external stimuli is close to T_∞, and no strict synchronization as in the case of the entrainment attractor is obtained. Both regimes are stable with respect to a small shift of the measuring point, which always constitutes the symmetry center of these attractor orbits [14].

More recently, this kind of local feedback control was also applied to rigidly rotating spiral waves [16, 17, 18], characterized by only one rotation period. In this case, only the resonance attractor was observed and mostly the trajectories of this attractor are epicycloids, i.e., their petals are directed inwards. However, it was reported in a numerical study [16] that very small resonance attractors may assume a hypocycloidal shape, i.e., with outward directed petals. This latter case has not yet been investigated in the laboratory, and we show in this letter that, in fact, hypocycloidal resonance attractors exist for rigidly rotating spiral waves and that their occurrence depends sensitively on the initial conditions chosen for the feedback signal. We investigate their dynamical features under the application of time delays. The results are corroborated by numerical simulations and compared with theoretical predictions.

Experimental method

The reaction was carried out in a petri dish (diameter, 5.5 cm) containing a thin layer (thickness, 0.30 mm) of silica gel [17]. The light sensitive $Ru(bpy)_3^{2+}$ catalyst was immobilized in the gel at a concentration of 4.2 mM. The BZ solution without catalyst was poured on top of the gel. After several minutes an equilibrium between liquid and gel was established and the following concentrations of reactants were reached: 0.20 M $NaBrO_3$, 0.17 M malonic acid, 0.39 M H_2SO_4, and 0.09 M NaBr. The gel and the solution were kept at a constant temperature of 25 ± 1 °C.

A wave front was broken with a spot (diameter, 1 cm) of intense light from a cold light source. As a consequence, the open ends of the wave begin to form a pair of spirals. One spiral was suppressed with the light spot to leave a single spiral in the center of the dish. This procedure defined the initial condition for all of the experiments. The gel in the petri dish was illuminated from below with a video projector and controlled by a computer. The pictures of the appearing oxidation waves were observed in transmitted light ($\lambda = 485$ nm), detected by a CCD camera and stored with a computer program. The spiral rotation was characterized by considering the trajectory of the spiral tip detected with image processing techniques, as specified in [3, 14, 17].

Results

For a given background light intensity $I_0 = 0.061 \pm 0.001$ mW/cm^2, the spiral tip rotates rigidly around a closed circle with a diameter of 0.36 ± 0.03 mm. The unperturbed rotation period is $T_u = 39.41 \pm 2.14$ s and the spiral wavelength is $\lambda = 1.92 \pm 0.10$ mm. The rigid rotation is disturbed by a sequence of short light pulses (amplitude A, duration 5 s), applied at the moment, when the wave front
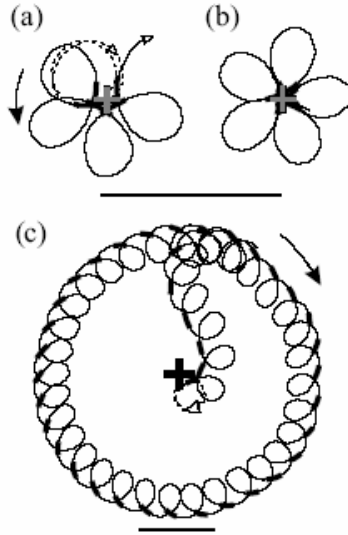
Figure 1: Hypocycloidal (a-b) and epicycloidal (c) resonance attractor of the rigidly rotating spiral. Initial distance between measuring point (cross) and unperturbed core center, R_0: (a-b) 0.093λ and (c) 0.155λ. $I_0 = 0.061$ mW/cm^2; $A = 0.050$ mW/cm^2. (a) Transient state of trajectory in (b), which is the stationary attractor several spiral rotations after starting the feedback. Thick segments indicate application of light pulses. The dotted line depicts the unperturbed spiral tip trajectory. Open and full arrows indicate the rotation direction of the spiral tip and the spiral core, resp. The radius of an attractor R_s is defined as the average of inner and outer radius of the looping trajectory. Scale bar: 1 mm.
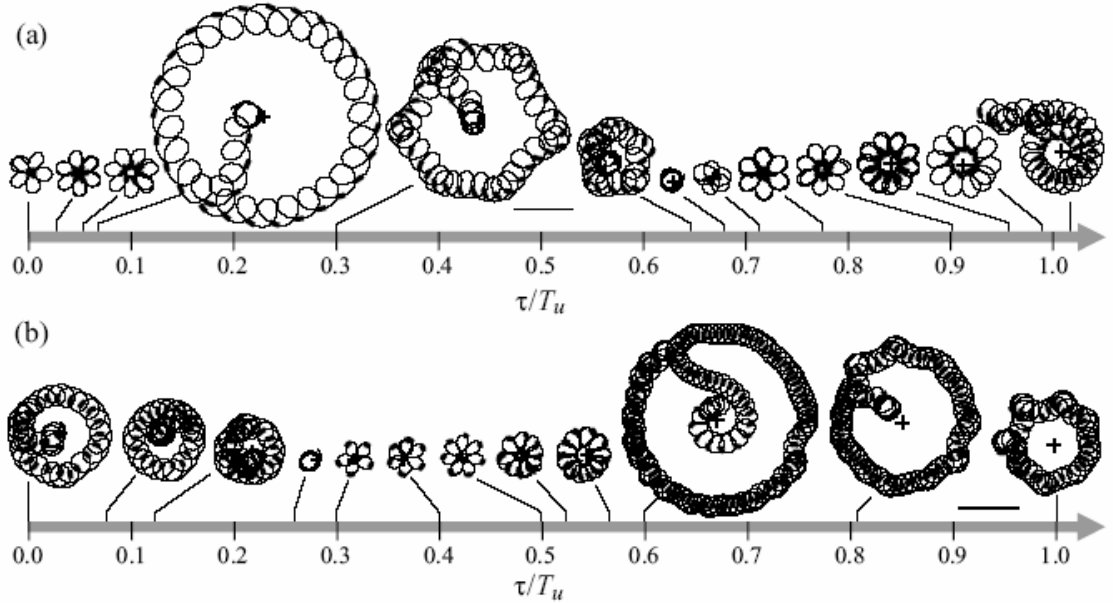

Figure 2: Trajectories of the spiral tip under variation of the time delay τ. (a) Positive pulse feedback with amplitude $A = 0.043$ mW/cm^2; (b) negative pulse feedback with $A = -0.031$ mW/cm^2, where $I_0 = 0.061$ mW/cm^2. The measuring point (crosses) was initially placed close to the unperturbed spiral core ($R_0 \leq 0.15\lambda$), except for the two orbits in (b) at $T_{mp}/T_u = 0.805$ and 1. Thick segments correspond to the application of light pulses. Scale bar: 1 mm.
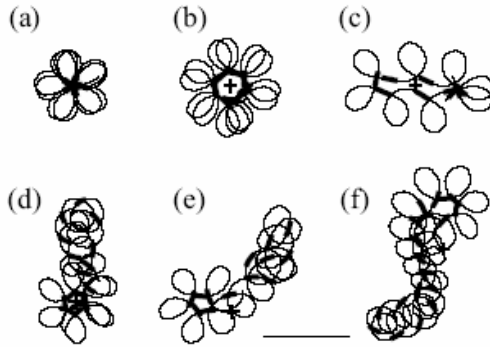
2

Figure 3: Trajectories of the spiral wave tip observed for large time delays τ, where $I_0 = 0.062$ mW/cm^2, $A = 0.091$ mW/cm^2. (a) $\tau/T_u = 0$, (b) $\tau/T_u = 1$, (c) $\tau/T_u = 2$, (d) $\tau/T_u = 3$, (e) $\tau/T_u = 4$, and (f) $\tau/T_u = 6$. Thick segments correspond to the application of light pulses. Scale bar: 1 mm.

passes through a preselected measuring point, or after some time delay τ. During the pulse the total light intensity I is either increased (positive pulse, $I > I_0$) or decreased (negative pulse, $I < I_0$).

The hypocycloidal resonance attractor is found to occur, if the measuring point is located very close to the core center of the unperturbed spiral (Fig. 1a), i.e., $R_0 \leq 0.15\lambda$. In this example the spiral wave tip asymptotically approaches a five-lobed hypocycloidal trajectory with its symmetry center coinciding with the measuring point (Fig. 1b). The ratio of the rotation period at the measuring point (T_{mp}) to the unperturbed period, T_{mp}/T_u, is 0.867 and the ratio of the attractor radius to the spiral wavelength, R_s/λ, is 0.117. The light pulses appear in the inner part of the loopy trajectory, and the drift direction of the spiral core is opposite to that of the tip rotation.

For $R_0 > 0.15\lambda$, the spiral tip describes an epicycloidal orbit centered at the measuring point, and we find $T_{mp}/T_u = 1.098$, $R_s/\lambda = 0.805$. The light pulses occur when the tip moves along the outer part of the loopy trajectory. The sense of rotation is the same for the spiral core and the spiral tip.

The dynamics of the hypocycloidal attractor was further studied after introducing a time delay τ into the feedback loop. Examples for positive ($A = 0.040$ mW/cm^2) and negative pulse feedback ($A = -0.031$ mW/cm^2) are shown in Fig. 2. Starting with $\tau = 0$ in Fig. 2a, the radius of the hypocycloidal resonance attractor increases with τ. This growth is accompanied by an increase of the number of lobes in the trajectory, i.e., 5, 6, and 7 lobes for τ/T_u=0, 0.026, 0.053, respectively. If the delay reaches a certain value ($\tau/T_u = 0.067$), a transition from the hypo- to the epicycloidal regime takes place. In the range $0.067 \leq \tau/T_u \leq 0.679$ only this regime is observed, although a very small R_0 was chosen. Note that the radius of the epicycloidal attractor decreases with τ in agreement with previous findings [16, 17]. At $\tau/T_u = 0.679$, however, this radius becomes so small, that the measuring point is finally located inside the spiral core and no light pulse is triggered any more. Then a further increase of τ brings the dynamics of the system back to the hypocycloidal regime, where the size of the attractor orbits increases with τ ($0.775 \leq \tau/T_u \leq 0.989$). Hypocycloidal attractor becomes again unstable at $\tau/T_u = 1.038$, consequently the dynamics switches, once more, to the epicycloidal regime.

Examples of hypocycloidal resonance attractors observed for negative pulse feedback are shown in Fig. 2b in the range $0.3 \leq \tau/T_u \leq 0.56$. Here, the pulses (indicated by thick segments) occur in the outer part of the hypocycloidal trajectory in contrast with the finding for positive pulse feedback (see Figs. 1a and 2a), where the pulses appear in the inner part. However, the time delay plays a similar role here, i.e., the radius of the attractor increases with τ.

Further instabilities of the hypocycloidal attractors are observed, when a prolonged time delay ($\tau/T_u > 1$) is introduced (Fig.3). A clear deviation from a circular symmetric attractor appears for $\tau/T_u = 2$ (extended hypocycloid, Fig. 3c). With increasing τ deviations become more pronounced: Apparently, the trajectories in Figs. 3d-f share a similar feature: they consist of a 'head' (circular, outward loops), and a 'tail' (extended, inward loops). The length of the tail increases with τ.

The dependence of the attractor radius R_s on the time delay τ is summarized in Fig. 4. The characteristics of the epicycloidal resonance attractors shown in this graph (diamonds and crosses) agree well with previous studies [16, 17]. The new results for the hypocycloidal resonance attractor are represented by squares and triangles (see caption).

Comparison with theory

A theoretical analysis has previously shown [16] that several stationary solutions of the attractor radius R_s exist for each value of the time delay τ and that the following equations should be satisfied:

3